Three-Dimensional Flow Separations on Aircraft and Missiles

DAVID J. PEAKE,* WILLIAM J. RAINBIRD,† AND EDWARD G. ATRAGHJI‡
National Aeronautical Establishment, National Research Council, Ottawa, Canada

William J. Rainbird; received his B.E.(Mech) at Canterbury University, Christchurch, New Zealand in 1947, and was awarded a Government scholarship to the College of Aeronautices, Cranfield, England, where he left in 1950 with a Post Graduate Diploma, with distinction, specializing in aerodynamics. After a year in Stockholm, Sweden working on transonic and supersonic wind-tunnel design at F.F.A., he returned to New Zealand and lectured at Canterbury University until September 1954. Returning to the College of Aeronautics, Cranfield that year, he was Lecturer in General and Experimental Aerodynamics for 3 years. Mr. Rainbird worked at the National Aeronautical Establishment, a Division of the National Research Council, Ottawa, from January 1958 to July 1970 and was a Senior Research Officer and Head of the High Speed Aerodynamics Section. In July 1970, Mr. Rainbird was appointed Professor of Engineering and Chairman of the Division of Aerothermodynamics, at Carleton University, Ottawa. In 1967, Mr. Rainbird spent a year's study and refresher leave at the University of California, San Diego, Department of Aerospace and Mechanical Engineering Sciences. He is a Fellow of the CASI, Associate Fellow of the Royal Aeronautical Society, Member of the AIAA, and was a Canadian Member of the AGARD Fluid Dynamics Panel from 1964–1969. His main field of specialization and interest in aerodynamics is in three-dimensional boundary layers and separation.

David J. Peake is a graduate of University of Bristol, England, Department of Aeronautical Engineering [B.Sc., 1960 (First Class Honors); M.Sc., 1962]. Concurrent with University training, Mr. Peake completed an Engineering Student Apprenticeship at National Gas Turbine Establishment, Pyestock, Farnborough, England, during 1956–1960. He remained at NGTE until May 1962 as Scientific Officer, working with Dr. Brian Stratford on the control of supersonic turbulent boundary layers with tangential air injection, and supersonic inlet design. Mr. Peake moved to National Research Council, Ottawa, Canada in May 1962, joining the Council's National Aeronautical Establishment in January 1964, in the High Speed Aerodynamics Laboratory. He worked with W. J. Rainbird in the investigation of three-dimensional separations in both subsonic and supersonic flow; transonic jet-flapped aerofoils, and axisymmetric turbulent boundary layers, all at high Reynolds numbers. Mr. Peake is studying for Ph.D. (part-time) at Carleton University, Ottawa and has membership in AIAA, RAeS and CASI. He has recently been awarded a Ph.D. from the University of Bristol for submitted published work.

Edward G. Atraghji is a graduate of University of London (B.Sc., 1962). He conducted research on slender delta wing configurations at Queen Mary College, London, between 1962 and 1966. He joined the National Research Council, NAE Division, High Speed Aerodynamics Laboratory, 1966. Topics of research have included the flows about various aircraft and missile configurations.

Introduction

THE integration of the load carrying, lifting and propulsion components of an aircraft or missile generates interfering pressure fields that often cause three-dimensional, boundary-layer separations. When the separation lines are inclined to the direction of the external mainstream, the resulting shear layers roll up to form comparatively steady vortex motions. Examples of such separated flows include those on slender wings, about upswept rear fuselages, about protuberances (bulbous wheel housings and boundary-layer diverters, for instance), and those produced by "favorable interference" from underwing power-plants. While the effect of these separations on drag may not always be significant, the problems associated with high-local, heat-transfer rates at reattachment areas and the interaction of the vortices upon downstream control surfaces are substantial.

The aerodynamic theories available to analyse these flows are few and inadequate. There is still no method to predict the growth and separation of a three-dimensional turbulent boundary layer (and the ensuing roll-up of the shear layer) on an arbitrary three-dimensional body even if the inviscid, interfering flowfields may be computed. In this review paper, some three-dimensional flow configurations are discussed where a good understanding of the viscous flow has been achieved.

Analogous to Howe's breakdown[1] of fluid mechanical problems connected with modern subsonic and supersonic aircraft, we may distinguish five overlapping areas of concern in our present study. The first and second, respectively, feature the prediction of the interfering inviscid flowfields, below which the three-dimensional, and usually, turbulent boundary-layer growth is required. If the pressure gradients are sufficiently adverse and sustained, we have in third part, that the three-dimensional boundary layer will converge, thicken and eventually separate along a line on the surface oblique to the local external stream direction. Fourthly, the three-dimensional separated shear layers are thrown clear of the body surface and roll up into vortical motions. When the separations are on a large scale, such as those occurring from the sweptback leading-edges of slender, lifting wings, or from upswept fuselages, then the nonlinear lift and the downstream decay of the vortices become important topics for investigation. The interaction of the vortices with propulsion intakes or lifting surfaces, and the likelihood of vortices bursting near the airframe are clearly detrimental to aircraft performance and control. The fifth problem area is

Received December 18, 1970. This review is an expanded version of an AIAA Paper 69-622, entitled "Some Problems of Three-Dimensional Flow Separation about Aircraft Components," that was presented at the AIAA Second Fluid and Plasma Dynamics Conference, San Francisco, Calif., June 16–18, 1969.

Index categories: Airplane and Component Aerodynamics; Jets, Wakes, and Viscid-Inviscid Flow Interactions.

* Research Officer, High Speed Aerodynamics Section. Member AIAA.

† Head, High Speed Aerodynamics Section; now Professor of Engineering, Carleton University, Ottawa. Member AIAA.

‡ Research Officer, High Speed Aerodynamics Section.

associated with relating the model scale three-dimensional viscous flowfields, as found in experiments, to those found on the full-scale aircraft or missile.

We shall concentrate upon the three-dimensional separations themselves on slender and not so slender bodies, on delta wings, on boundary-layer diversion systems, and on some flows in proximity to propulsion intakes.§ Before doing so, however, let us review briefly some available techniques for computing interfering inviscid flowfields.

A method to predict the interfering inviscid flowfields about arbitrary bodies in subsonic flow has been developed by A. M. O. Smith and his team[3] at McDonnell-Douglas, by enlisting the aid of large storage digital computers. The method cannot be used for three-dimensional lifting configurations, nor of course for assessing total drag. Useful calculations have been performed to investigate the pressure distributions in a wing/fuselage junction, about a DC-8 wing/pylon/nacelle and around a DC-9 fuselage/pylon/nacelle. Where compressibility effects were important, a Goethert transformation was employed. The agreement between computed and experimental pressure distributions was usually satisfactory in regions where the adverse pressure gradients were not too steep, and as a consequence, where three-dimensional separation effects were small.

A method of designing a swept wing-body combination to produce low wave drag and shockless flow has been proposed by Bagley.[4] Linear theory was used to compute the individual contributions from the wing and the body, to the flow in the wing-body junction. Hunt's experiments[5] with free-flight models, tested at Mach numbers between 0.8 and 1.5 at wing chord Reynolds numbers up to 10 million, indicated that the method was adequate to define the junction velocity distribution and to predict shockless flow. The tests were confined, however, to a wing with a symmetrical section at zero lift. Notwithstanding the claimed accuracy of the method, a close inspection of the differences between the prescribed and measured pressure distributions in the wing/body junction shows them to be large ($\Delta C_p = 0.1$ to 0.15) near the leading-edge, perhaps as a result of a three-dimensional, protuberance-type separation in the junction.

Woodward[6] has produced a versatile method, representing a wing-body combination by a system of source, doublet and vortex singularities, in an analagous way to the authors of Ref. 3. The essential difference is that Hess and Smith satisfy the flow boundary conditions on the surface of both the wing and the body, whereas Woodward satisfies the wing boundary conditions on the body and on only the wing camber surface. This linearization of the boundary conditions apparently does not introduce appreciable error in the results with thin wings ($t/c \doteq 0{\cdot}1$). Some discrepancies are again shown between the computed and measured body pressures in the vicinity of the leading-edge as a result of three-dimensional viscous effects.

A good survey of current analytical methods in aircraft aerodynamics is contained in the published proceedings of a symposium held at Ames Research Center in 1969 in which the wing-body problem is further discussed by Carmichael et al.[7] and Woodward et al.[8] Of particular relevance to the present context is a theoretical study of the nonlinear vortex flows on slender, wing-body combinations by Levinsky and Wei[9] and their results will be introduced in a later section. An evaluation of recent theories and experiments on aerodynamic interference, with particular attention paid to wing/body and wing/body/tail flows, airframe/propulsion interactions and airframe/stores' interactions, is published in Ref. 63.

In summary, we may quote Küchemann[10] in a recent paper on the wing/body problem, who states succinctly "many problems still remain unsolved; they arise mainly from the effects of viscosity and compressibility. A satisfactory theoretical treatment of the real flow past a given configuration of complex shape does not yet appear to be within reach and the establishment of a reliable and practical design method will require a considerable and determined effort."

§ Korkegi,[2] in a recently published paper, gives an excellent review of the viscous interactions associated with high-speed flight paying particular attention to the high-heating rates due to flow reattachment.

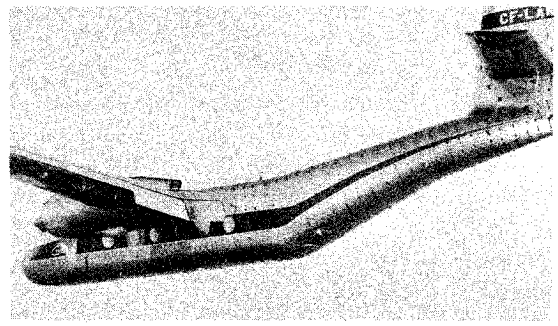

Fig. 1 Upswept fuselage flow on "Caribou" aircraft with flaps deflected. (Courtesy of de Havilland Aircraft of Canada, Ltd.)

Body Flows

Fuselage

Let us commence our set of illustrative examples with reference to flows about aircraft fuselages. The translation[11] of Multhopp's article on fuselage aerodynamics originally published in 1941 opens its introduction with: "one notoriously neglected phase in the aerodynamics of aircraft is that of the fuselage." Unhappily, this statement is still more or less true today, mainly because of the difficulties in dealing with the mutual interference generated by attaching to the fuselage, the wings, tail unit and engine nacelles (where applicable) and the lack of understanding of viscous and inviscid three-dimensional flowfields. Haines[12] attributes the disappointingly high drag of modern transport aircraft, in part, to the maintenance of the full diameter pressure cabin well aft; the consequence of which is rapid boat-tailing and upsweep of the rear fuselage for ground clearance on takeoff. Frequently, the drag rise is found to occur before the projected cruise Mach number is attained. Such a phenomenon is associated with local supersonic flow and shock waves in the regions adjacent to the nacelle/pylon/body or wing junctions. In addition as a result of three-dimensional, boundary-layer separations, so-called 'excrescence' drag can be as high as 8–24% of the aircraft profile drag at cruise. Appropriate filleting of the excrescence junction with the airframe, done on an ad hoc basis, can significantly reduce this drag contribution.

The flows about the upswept rear fuselages of cargo transport aircraft have been investigated at NAE, and were substantially reported in Refs. 13–15. Current available calculation procedures were also assessed,[14,15] whereupon it was judged that none of the methods investigated was suitable to compute the gross effects of the three-dimensional inviscid and viscous flowfields.

A typical, complex, upswept fuselage flow is shown on Fig. 1. Here, one may observe from the directions of the tufts on the upswept rear fuselage of a de Havilland of Canada "Caribou" aircraft that large cross-flow angles are present and that separation is occurring along the lower flanks of the afterbody. The boundary-layer cross flow is exaggerated in this instance by the large wing flap angle, but even under cruise conditions for this class of rear-loading aircraft, three-dimensional separations are sometimes present.

The maintenance of a low-cruise drag is especially important for long range transport aircraft. For instance, one count of cruise drag (a ΔC_D of 0.0001 and 0.4% of the total cruise drag) is said to reduce the long range mission payload of the Lockheed C-5A Galaxy by about 1%.[16] This level of resolution on measured drag is claimed in some meticulous wind-tunnel tests with a model of the Super VC-10.[17] It was found possible to obtain axial force measurements repeatable and consistent to within $\Delta C_D \doteq 0.00005$. Other systematic errors in the tests related to pressure measurements, incidence, flow direction and sting interference, increased ΔC_D to about 0.00025—still a fine achievement.

The next illustration in Fig. 2 exemplifies the pattern of surface

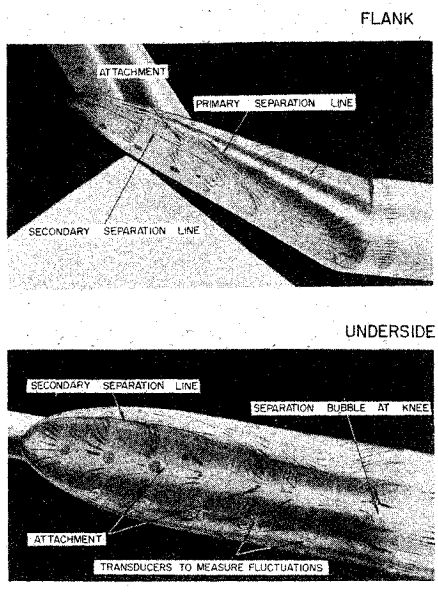

Fig. 2 Separation and attachment lines on a "beaver tail" afterbody at an upsweep angle $\beta = 20°$.

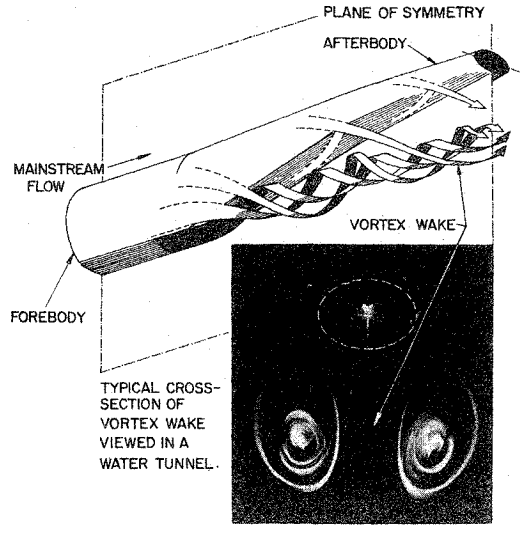

Fig. 4 Vortex wake beneath an upswept rear fuselage.

shear stress trajectories obtainable with the oil dot flow visualization technique, on the upswept afterbody of a research model tested in the NAE 5 × 5-ft blowdown wind tunnel. The tests were conducted at a Mach number of 0.73 and at a Reynolds number of 30 million based upon the 40-in. fuselage length. The fuselage boundary layer was turbulent and was not tripped by any artificial means.

The straight "beaver tail" shape with elliptical cross-sections is not untypical of the STOL aircraft type with rear-loading capability that has been manufactured in Canada. The upsweep angle was adjustable on this NAE model, and in Fig. 2, it was set at a large value of 20°. Supplementing the oil flow photographs are the afterbody section pressure distributions on Fig. 3 that aid in the synthesis of the afterbody flow. Except at those cross sections furthest downstream, we note a steep but favorable transverse pressure gradient from the top of the fuselage towards the flank. Following the favorable pressure gradient the limiting streamlines sweep down over the flanks of the afterbody. A re-examination of Fig. 2, however, shows that when the pressure gradient reverses sharply, the limiting streamlines converge and coalesce, forming primary separation lines beginning some distance back along the rear fuselage. The turbulent shear layers springing from the primary separation lines roll up to form vortex motions illustrated on Fig. 4. A pair of primary vortices develop, standing clear of the surface, which induce the external flow passing over them to attach at the underside center-line of the fuselage. The regions of high-suction pressure beneath the vortices are clear from Fig. 3; it is this suction on the upswept aft-facing surface that may produce large nose-up pitching moments, high drag at cruise, as well as undesirable loadings on the aft-fuselage doors. Measurements of peak-to-peak amplitudes of pressure fluctuations on the afterbody by means of surface pressure transducers, in the vicinity of the secondary separation line, yielded values 10 to 20 times greater than a typical rms value for turbulent boundary-layer surface pressure fluctuations. Even for extreme upsweep angles, there was no evidence of low-

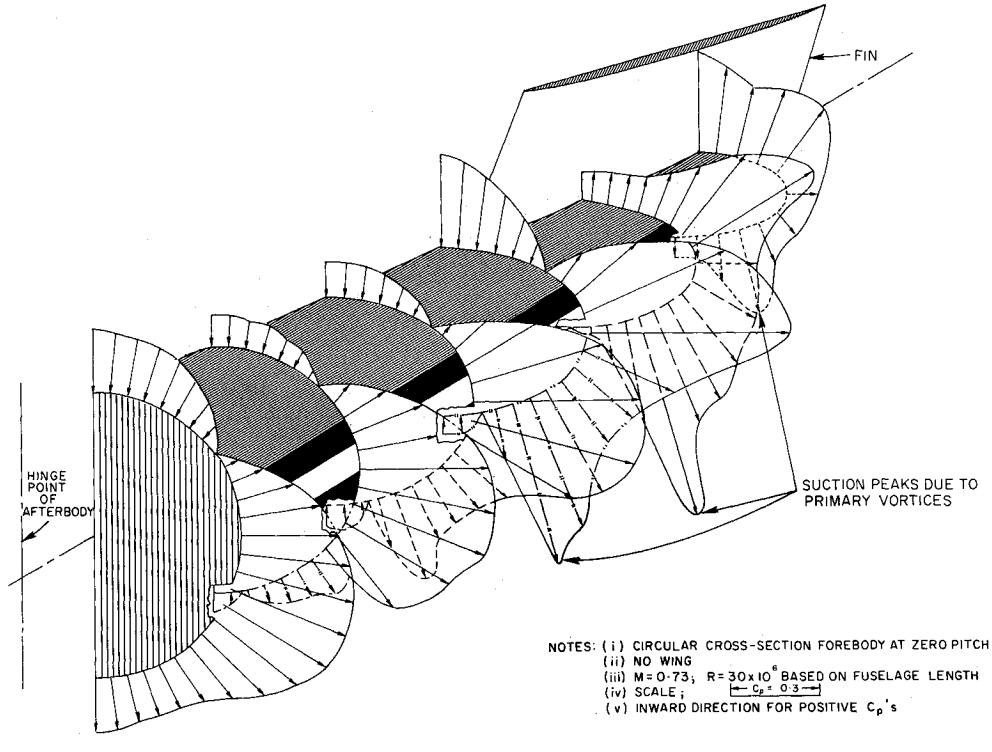

Fig. 3 Distributions of pressure coefficient on a "beaver tail" afterbody at an upsweep angle $\beta = 20°$.

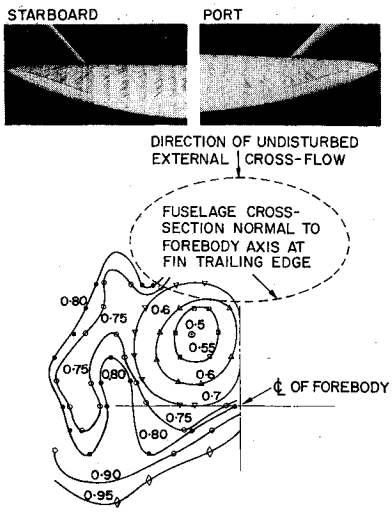

CONTOURS OF PITOT PRESSURE COEFFICIENTS, C_{p_0}, JUST DOWNSTREAM OF AFTERBODY TIP, VIEW LOOKING UPSTREAM.

Fig. 5 9° upswept fuselage at $M_\infty = 0.3$, $\alpha_{FB} = -15°$, and $R_L = 22 \times 10^6$.

frequency periodic vortex shedding at the high-test Reynolds numbers.

Figure 5 demonstrates the afterbody flow patterns and contours of constant Pitot pressure in a vortex wake beneath another, but typical, 9° upswept afterbody at Mach 0.3 and at a Reynolds number of 22 million based upon the 39.4 in. model length. Such rotational flow in the wake may also affect the extraction and the dropping capabilities of cargo by parachute from an upswept fuselage aircraft.[18]

An inviscid flow, modified slender body calculation that had been used with relative success previously,[19] gave afterbody pressure distributions for the NAE model that described the trends of the experimental results but did not predict the transverse pressure gradients. The large discrepancies were due to the afterbody viscous flow and vortex wake as well as the "protuberance type" fin pressure field, neither of which was adequately represented in the calculations. The cross-flow drag approach[20,21] was inappropriate in this instance because the potential force term that is proportional to the rapidly changing afterbody cross-sectional area (and which cannot be neglected) exceeded the viscous cross-flow force term.

The overwhelming influence of the vortex wake poses the question of whether it can be represented in a theoretical model. An inviscid flow computation treating the rolling-up of a vortex sheet from a given separation line, such as that developed, for example, by J. H. B. Smith[22] for a slender delta wing at incidence, would not appear amenable to modification for the upswept fuselage case. In the first place, the conicity of the flow that Smith considers would not apply to the flow about the fuselage; secondly, the initial separation position of the afterbody viscous flow is unknown and may not at this time be computed with confidence, because of the infant state of three-dimensional turbulent boundary-layer theory. Even if the separation positions were known, there would be a third difficulty in identifying the initial strength and direction of the free shear layers.

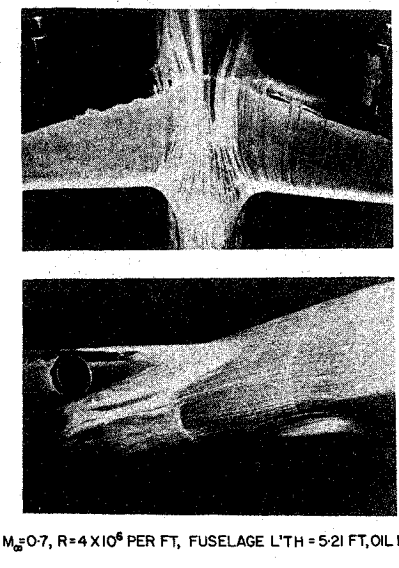

M_∞=0·7, R=4 X10^6 PER FT, FUSELAGE L'TH = 5·21 FT, OIL FLOW

Fig. 6 Lockheed C-5A junction oil flow visualization.

The analysis of the upswept fuselage flow, therefore, presents many difficulties, added to which are the complications of other three-dimensional flow separations passing downstream from the wing root junction and from about bulbous undercarriage housings. (A well-considered airplane from the point of view of junction design is the Lockheed C-5A, Fig. 6 illustrating that both the wing-body and undercarriage-body fairings produce smooth three-dimensional boundary-layer flows without any evidence of three-dimensional separation.) Hence, while we have a good qualitative understanding of fuselage flows, we are far from a position of being able to predict their inviscid or their viscous flow characteristics with a high degree of certainty.

Ellipsoid of 6:1 Fineness Ratio

Next, we look at the comparatively simple flow about a prolate spheroid generating lift at subsonic speeds. Some tests with a sting-mounted ellipsoid¶ of 6:1 fineness ratio and length 54-in. were performed[23] in the NAE 5 × 5-ft wind tunnel at Mach numbers of 0.3 and 0.74. A Reynolds number of 44 million based on the body length ensured turbulent boundary-layer conditions. No gross changes were noted between the results at the two Mach numbers, so that we will restrict our remarks to the $M_\infty = 0.74$ tests. The 6:1 fineness ratio is not a slender body in the literal sense of the term, but a corresponding flow situation would exist, of course, about an ellipsoid of larger fineness ratio at a reduced angle of incidence (that is, at the same relative incidence).

Measurements of body static pressure, Preston tube impact pressures and surface oil streak directions were made in an incidence range 0 to 25°. The Preston tubes were aligned nominally with the local surface shear stress direction using a previously obtained oil streak pattern. Notwithstanding the three-dimensionality of the flow, Preston's two-dimensional calibration[24] was applied to reduce the surface tube data to skin friction form.

Figures 7 and 9 present the circumferential static pressure distributions at various axial stations along the ellipsoid, at angles of incidence α of 10° and 25°. For comparison, a calculation of the exact incompressible inviscid flow about an ellipsoid, originally due to Lamb and Munk and presented again in Refs. 25 and 26 (but suitably corrected for compressibility[27]) is set against each measured pressure distribution. Figure 7, at $\alpha = 10°$, where the flow is everywhere attached except over a small region of the leeward afterbody, demonstrates good resemblance between the slopes of the pressure distributions despite a consistent difference in absolute level between measured and calculated results. This difference is greater than the maximum estimated measurement error, $\Delta C_p = \pm 0.024$, while Cloutier[28] noted an even larger discrepancy in pressure between theory and some experiments at low speed where there was a mixed viscous flowfield of laminar, transition, and turbulent boundary layers at $R_L \doteq 3$ million. These respective discrepancies at high and low Reynolds numbers are in contra-distinction to the good agreement obtained by Matthews[29] between his Prandtl-Glauert theory and measurements at R_L between 5 and 8 million at small angles of incidence. On the other hand, Matthews did eliminate his low Mach number measurements because of considerable scatter in the pressure coefficient results and moreover, did not support his higher Mach number tests with a quoted measurement error.

¶ The model was kindly supplied by E. Eichelbrenner of Laval University, Quebec City, Canada.

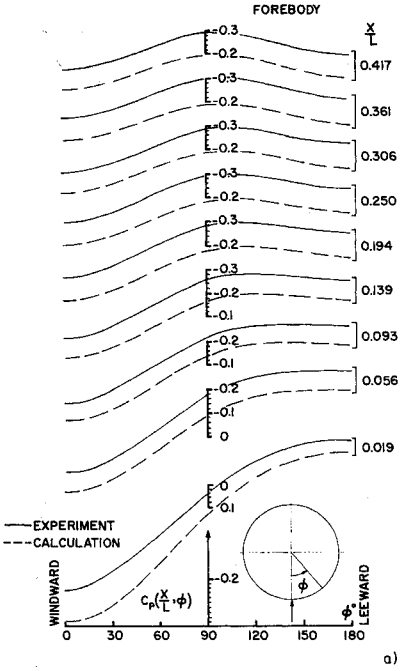

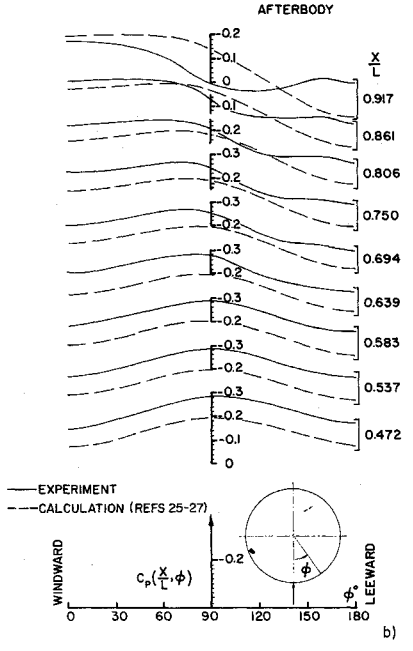

Fig. 7 Circumferential pressures on 6:1 ellipsoid at $\alpha = 10°$, $M_\infty = 0.74$, and $R_L = 44 \times 10^6$.

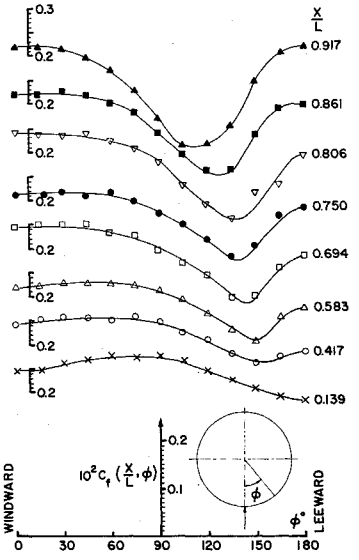

Fig. 8 Circumferential variation of skin friction at various distances along axis of 6:1 ellipsoid at $\alpha = 10°$, $M_\infty = 0.74$, and $R_L = 44 \times 10^6$.

The skin-friction results, in keeping with the pressures shown on Fig. 7, indicate a slow reduction of skin-friction coefficient C_f with distance along a generator (except at the nose and tail). When the skin-friction distributions are viewed alternatively in the circumferential sense, large gradients are displayed (Fig. 8) with a pronounced reduction in C_f towards the leeward generator that is consistent with a thickening boundary layer. Increasing the incidence to a value greater than 15° causes the circumferential pressure gradients to become progressively more adverse, completely swamping the axial gradients (as in the case of the upswept fuselage). Accordingly, a three-dimensional separation region spreads forward, until at $\alpha = 25°$ almost the entire leeward surface is experiencing the gross effects of one or more three-dimensional separations. Figure 9 illustrates the high suction peaks on the leeward side beneath the rolled-up shear layers resulting from the primary separations, along with the positions of the separation and attachment lines that are symmetrical about the pitch plane of the ellipsoid.

Our understanding of the high-incidence flow case is enhanced by drawing the calculated and experimental isobar patterns on a distorted unwrapping of the ellipsoid surface, see Fig. 10. The favorable and adverse circumferential pressure gradients are denoted, respectively, by open and shaded arrows. From the calculated inviscid pressure field,[25-27] one would expect separation to occur somewhere on the leeward side of the minimum pressure line. Affirmation of this premise is provided by overplotting the measured isobars with the separation lines deduced from the equivalent oil flow visualization study.

The inner boundary-layer behavior, in fact, is shown on Fig. 11 in terms of the pattern of surface shear stress trajectories found from oil streak flow visualization. The heavy lines mark the experimental minimum pressures, inboard of which the turbulent boundary layer separates after it encounters the adverse circumferential pressure gradient (see Fig. 10, also). The flow with separation again reveals its symmetry as it did in the case of the upswept fuselage, an attachment line along the leeward generator ($\phi = 180°$), and a secondary separation extending well forward and outboard of this attachment, being additional distinctive flow features. In contrast with the simpler three-dimensional separation on cones that has also been studied at the NAE,[30-32] these more general body flows exhibit substantial lengthwise effects although the circumferential pressure gradients still predominate. As a rule, it is unclear where convergence and thickening of the three-dimensional, boundary-layer stops and separation commences. Again, however, it does appear that three-dimensional separation is a gradual, nonviolent process, with no low-frequency pulsation of the separated flow at these high Reynolds numbers.

To emphasise the nonlinear lift contribution generated by the lee-side vortices, Fig. 12 shows the experimental and computed sectional normal force coefficients. Here, the systematic discrepancies in absolute level between the measured and the calculated pressure coefficients are effectively removed in the summing around the surface. From these integrated results, we are able to recapitulate that the viscous effects at $\alpha = 10°$ are relatively small; at $\alpha = 25°$, on the contrary, the normal force coefficient is substantially increased by the induced suction pressures from the lee-side vortices downstream of $x/L \doteq 0.2$, this phenomenon being analogous to the flow over sharp-edged slender wings.

Long, Pointed Slender Bodies

The following section enlarges upon the discussion of 'separation on long bodies' that was published in Ref. 30. As we noted there, the body of a missile or rocket is prone to the effects of three-dimensional separation once it departs from a zero incidence flight trajectory. One may regard the long cylindrical body as a cone of zero included angle, and so for any small angle of incidence, the *relative* incidence is large, and separation is inevitable somewhere along the body, provided it is long enough.

To improve our understanding of the flow characteristics about a family of long, pointed slender missile configurations at subsonic and supersonic Mach numbers (0.5, 2.0, and 3.5) a series of

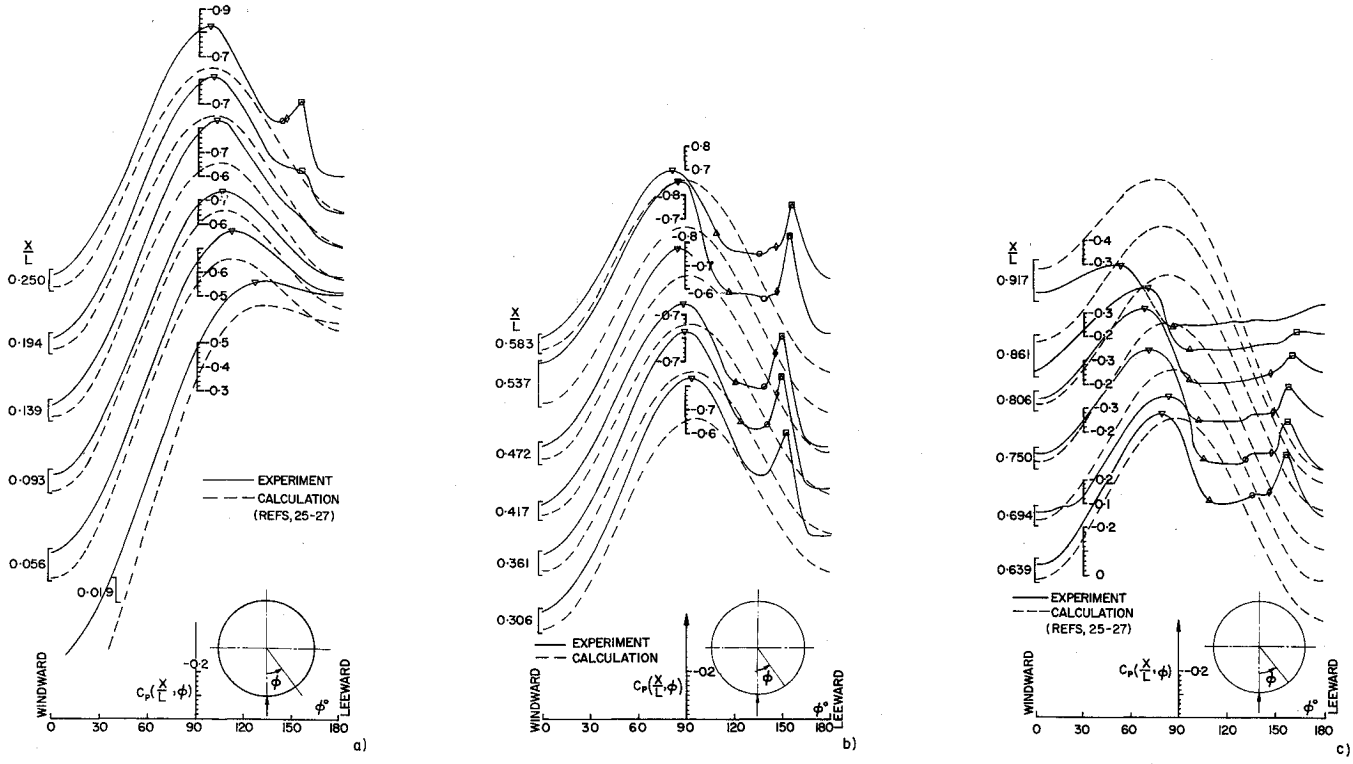

Fig. 9 Circumferential pressures on 6:1 ellipsoid at $\alpha = 25°$, $M_\infty = 0.74$, and $R_L = 44 \times 10^6$. ∇—minimum pressure, Δ—primary separation, ○—secondary attachment, ◇—secondary separation, □—suction peak from primary vortex.

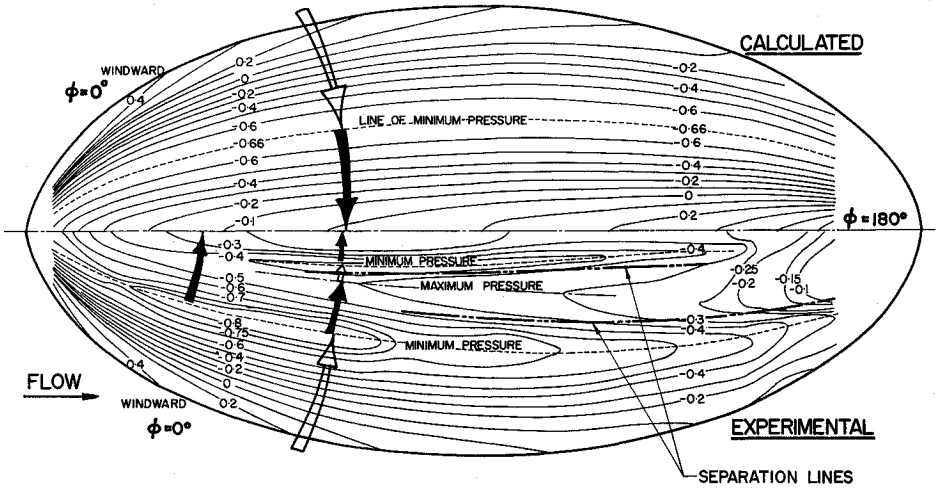

Fig. 10 Isobars on 6:1 ellipsoid at $\alpha = 25°$, $M_\infty = 0.74$, and $R_L = 44 \times 10^6$.

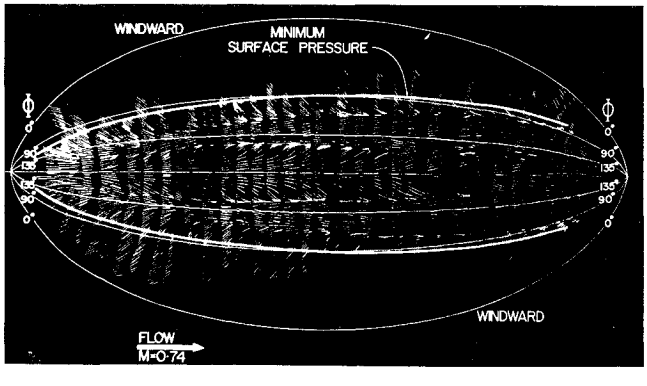

Fig. 11 Oil dot surface flow visualization on 6:1 ellipsoid at $\alpha = 25°$, $M_\infty = 0.74$, and $R_L = 44 \times 10^6$.

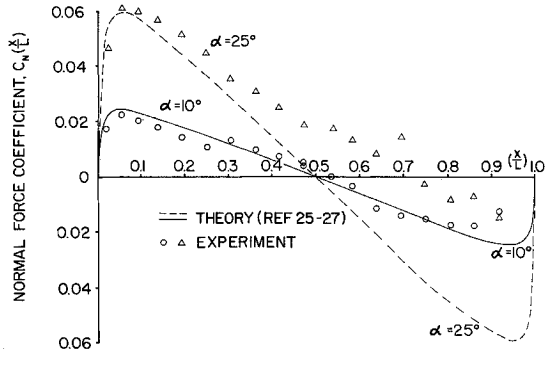

Fig. 12 Distribution of normal force along 6:1 ellipsoid; $\alpha = 10°$ and $25°$, $M_\infty = 0.74$, and $R_L = 44 \times 10^6$.

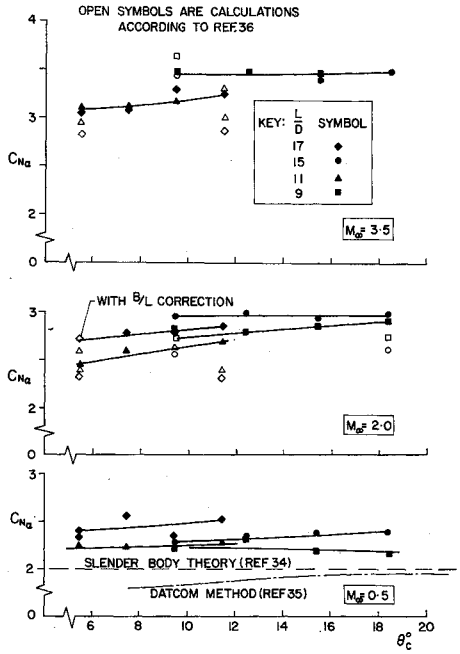

Fig. 13 Low-incidence performance of long pointed slender bodies. Normal force slope vs seminose angle at $M_\infty = 0.5$, 2.0, and 3.5 at $R_D = 1$ to 4×10^6.

tests was conducted[33] in the NAE 5 × 5-ft wind tunnel at Reynolds numbers R_D varying between 1 and 4 million, based upon the cylinder body diameter D of 4 in. The models differed in nose shape and length of afterbody. The former consisted of cones and parabolic ogives whose geometries are listed below on Table 1. Each nose could be attached to a cylindrical afterbody length of either 6D or 12D, but no stabilizing fins were affixed in any of the tests.

Three distinct flow régimes were detected during the pitching of any given configuration concordant with no three-dimensional separation, symmetric separation and asymmetric separation. For all that, the nature of the separations again appeared orderly and nonviolent up to angles of incidence of 25°.

For low angles of incidence (typically up to $\alpha = 3°$) where there was attached flow, the slope of the normal force incidence plot C_{N_α} increased with Mach number and seminose angle θ_c (see Fig. 13). The effect of slenderness ratio, L/D, was less clear, although at $M_\infty = 0.5$, the trend was established of increasing

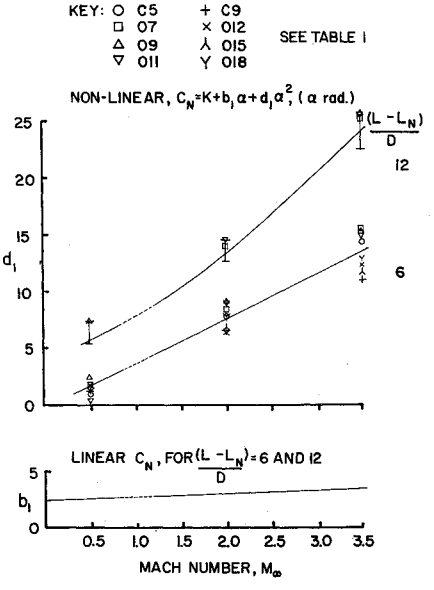

Fig. 14 Linear and nonlinear lift on long pointed slender bodies at $R_D = 1$ to 4×10^6.

Table 1 Details of long, pointed, slender bodies

CONFIGURATION	SEMI-APEX ANGLE θ_c	NOSE LENGTH $\frac{L_N}{D}$	AFTERBODY LENGTH $\frac{L - L_N}{D}$	m
C5-12D	5°43'	5	12	1
07-12D	7°36'	5	12	4/3
09-12D	9°28'	5	12	5/3
011-12D	11°19'	5	12	2
C9-12D	9°28'	3	12	1
012-12D	12°31'	3	12	4/3
015-12D	15°31'	3	12	5/3
018-12D	18°26'	3	12	2
C5-6D	5°43'	5	6	1
07-6D	7°36'	5	6	4/3
09-6D	9°28'	5	6	5/3
011-6D	11°19'	5	6	2
C9-6D	9°28'	3	6	1
012-6D	12°31'	3	6	4/3
015-6D	15°31'	3	6	5/3
018-6D	18°26'	3	6	2

C=CONE, O=OGIVE.

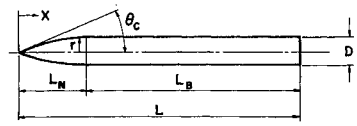

NOSE CONTOUR: $\frac{r}{D} = \frac{1}{2}\left[1-\left(1-\frac{X}{L_N}\right)^m\right]$

C_{N_α} with L/D. Calculations using slender body theory,[34] the USAF "Datcom" data sheets[35] and the method due to Öhman[36] are also included. As a generalization, the theories would seem to underpredict C_{N_α} at a given seminose angle and slenderness ratio.

In the range of incidence, characteristically $\alpha = 3°$ to 11°, there is symmetric three-dimensional flow separation from the leeward side of the missile, which develops in a way resembling that about the ellipsoid discussed earlier. The induced suction pressures from the rolled-up shear layers generate a large nonlinear lift component, but no sideforce. Representing the normal force coefficient by a quadratic in α

$$C_N = K + b_1 \alpha + d_1 \alpha^2$$

where K only removes the experimental uncertainty in the true incidence measurement, Fig. 14 illustrates the increase in the coefficients b_1 and d_1 with both Mach number and slenderness ratio with less importance attributable to the seminose angle θ_c. Notwithstanding, the more slender ogives (07, 09, and 011 on Table 1) would appear to generate a larger nonlinear lift throughout the Mach number range and for both lengths of afterbody.

Thus at moderate angles of incidence, three-dimensional separation occurs symmetrically, with a pair of vortices trailing back along the body. At higher angles of incidence, asymmetric flow conditions can occur causing large side forces to be developed. The asymmetry is influenced initially by the conditions at the pointed nose and stream Mach number; and once begun, by the afterbody length. The direction of the side force changes with incidence but is repeatable for the same model geometry in a given wind-tunnel test. Increasing the Reynolds number would appear to delay the onset of asymmetry. Figure 15 illustrates the

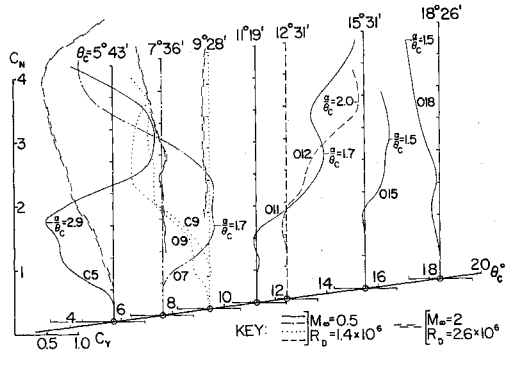

Fig. 15 Influence of seminose angle θ_c on side force (C_Y) – normal force (C_N) polars for afterbody length of 12D.

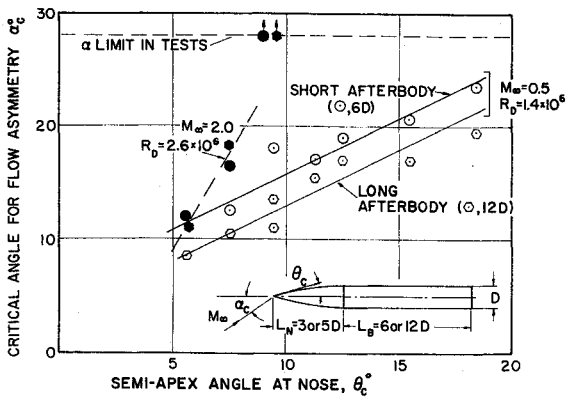

Fig. 16 Critical angle of incidence for onset of flow asymmetry about long pointed slender bodies.

magnitude of the mean side force coefficient C_Y with respect to the normal force coefficient C_N as the model incidence is increased, for all of the nose shapes tested with the 12D afterbody length. Oscillations in sideforce, peak-to-peak amplitudes being as high as ± 0.3 at $\alpha = 25°$, were superimposed upon the mean C_Y levels. We note that increasing either the seminose angle or Mach number, for angles of incidence up to about 27°, resulted in a reduction of the side force. In fact, at $M_\infty = 2$ when θ_c exceeded 10°, and for all configurations at $M_\infty = 3.5$, no measurable side force was obtained. Similar results have also been measured on circular cones,[31] the re-establishment of symmetrical flow being associated with shock waves present in the cross flow.

Figure 16 presents the critical angle for flow asymmetry (judged by the side force exceeding, say, 5% of the normal force) plotted against the nose semiangle θ_c. As before, we confirm that the onset of flow asymmetry is delayed by increasing θ_c and Mach number. In addition, one also notes the effect of the longer afterbody in hastening the asymmetry simply because the asymmetry has an increased time in which to develop along the 12D length.

Finally, oil dot flow visualization again permitted the locations

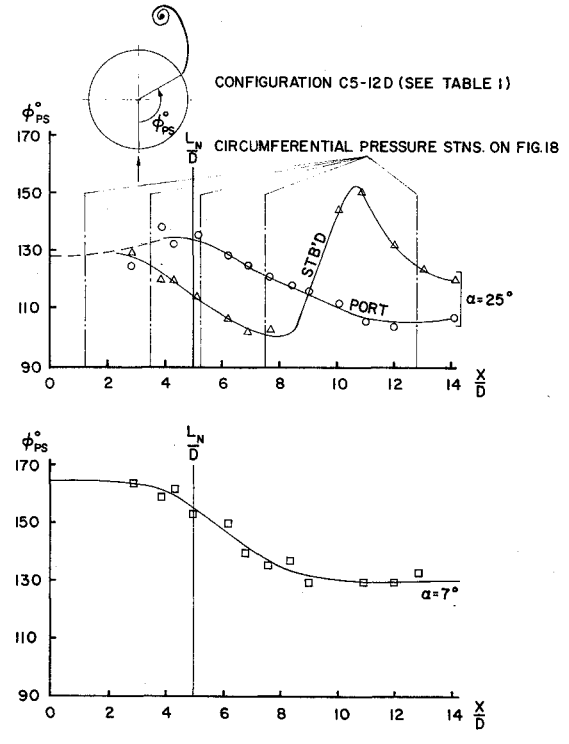

Fig. 17 Asymmetric and symmetric primary separation angles on a 5.7° cone-cylinder at $M_\infty = 0.5$ and $R_D = 1.4 \times 10^6$.

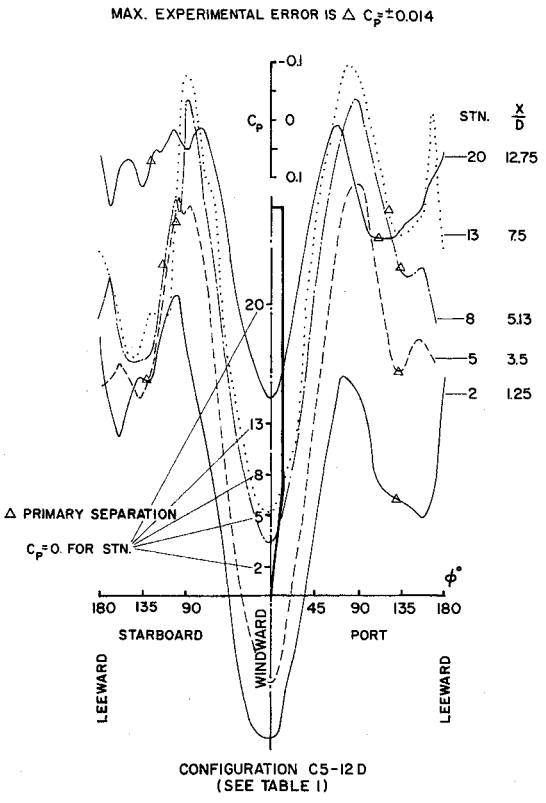

Fig. 18 Circumferential pressures on a 5.7° cone-cylinder at $\alpha = 25°$, $M_\infty = 0.5$, and $R_D = 1.4 \times 10^6$.

of the three-dimensional separations to be measured. On Fig. 17, at $M_\infty = 0.5$, the circumferential positions of the primary separation lines are plotted for the most slender (C5–12D) cone-cylinder configuration at $\alpha = 7°$ amd 25°, corresponding to symmetric and asymmetric flow separation ($C_Y = -0.7$, compare with Fig. 15). Supporting the asymmetric case are the corresponding circumferential pressure distributions[37] on Fig. 18, where the primary separations and induced suction peaks are indicated.

Slender Wings and Wing-Body Combinations

The best known and most studied example of three-dimensional separation occurs along the leading edges of lifting slender wings. For slender sharp-edged delta wings, a number of nonlinear but conical inviscid flow theories have been developed that account for the vortex sheets springing from the leading edges and coiling above the upper surface of the wing. The Mangler and Smith[22] theory is perhaps the most sophisticated; however, such conical methods neither account for compressibility nor for the unloading

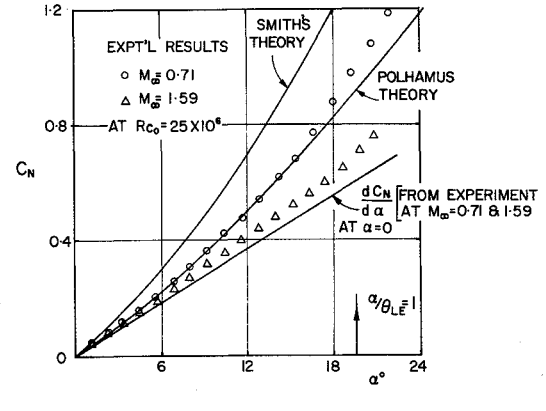

Fig. 19 Over-all normal force on 70° delta wing in subsonic and supersonic flow.

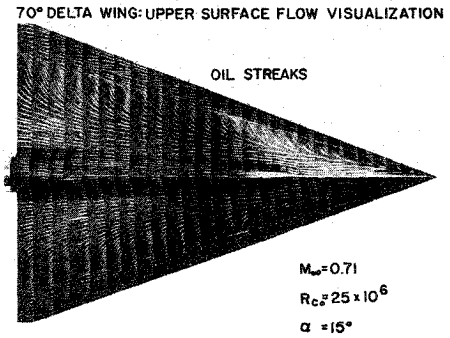

Fig. 20 Upper surface oil flow visualization on 70° delta wing at incidence in subsonic flow.

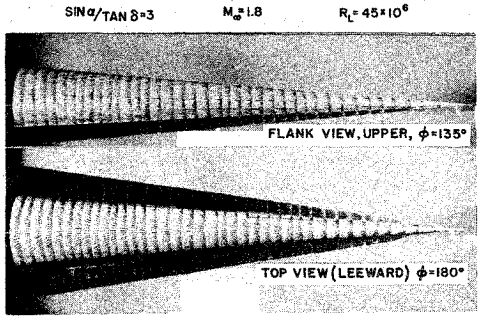

Fig. 22 Surface oil flow visualization on 5° cone with 75% strake wings in supersonic flow.

of the wing at a subsonic trailing-edge. Polhamus,[38,39] on the other hand, has produced an "over-all" theory which assumes that due to separation, the leading-edge suction force is rotated 90° into a direction normal to the wing chord plane, thus giving a nonlinear component to the normal force. While no theoretical proof of this method has been established, there is no doubt that it works successfully.

Figure 19 shows the over-all normal force measured on a sharp-edged 70° delta wing under high Reynolds number conditions, $R_{c_0} = 25$ million, based on the wing-root chord of 30 in. The test Mach numbers in the NAE 5 × 5-ft wind tunnel were 0.71 and 1.59. The agreement of the subsonic measurements with the Polhamus theory is excellent up to a relative incidence $\alpha/\theta_{LE} = 1$ in contrast with Smith's[22] conical flow theory, which overpredicts the normal force. One should also note that there is a marked decrease in the nonlinear lift at supersonic speeds even though at $M_\infty = 1.6$, the wing is still slender: $(M_\infty{}^2 - 1)^{1/2}$ (semi-span)/length = 0.43. Squire et al. in Ref. 40 have noted that this decrease is associated with a flattening of the leeward side vortex structure.

Figure 20 provides details of the surface shear stress trajectories on the upper surface of the delta wing at $M_\infty = 0.71$ and $\alpha = 15°$. The flow sweeping over the primary vortex (resulting from the leading-edge, three-dimensional separation) attaches to the surface and from this attachment line a new boundary layer grows along and across the wing, finally meeting an adverse pressure gradient and separating from an almost conical secondary separation line inboard of the leading edge. A stream surface sweeping over the secondary vortex attaches along the line of oil streak divergence between the leading edge and the secondary separation, new boundary-layer flow from which feeds the shear layers springing from both the primary and secondary separations.

More complex but still conical cases have been treated by Levinsky and Wei,[9,41] using essentially the same formulation as Mangler and Smith, but accounting for a conical body. Some measurements that have been made at NAE using a 5° semiapex angle cone with 75% strake wings are shown on the next illustration in Fig. 21 and are compared with linear, and Levinsky and Wei's nonlinear theory. Up to relative incidences of about 2, the experimental results at $M_\infty = 0.71$ and 1.80 agree closely with each other, indicating that the trailing-edge effects are perhaps small for this slender configuration. Nonetheless, at higher relative incidences for the $M_\infty = 1.8$ case, conically mixed flows occur, i.e. flows including conically subsonic and transonic regions, the latter being terminated by internal shock waves.

While the Levinsky and Wei nonlinear theory takes account of the leading-edge separation, it does not include the effects of the many other separations that exist around such wing-body combinations. Figure 22 demonstrates the oil dot surface flow visualization on the same 5° cone with 75% strake wings at a relative incidence of 3 in a stream of Mach number 1.8. On the upper surface of the cone, following the attachment of the stream surface induced by the leading-edge vortices, strong body separations are evident. The upper surface wing flow being inward rather than outward (the latter customary for a delta wing flow with separation) is apparently dominated by vortices of opposite sign shed from the body separation lines. In addition, the view of the upper flank, $\phi = 135°$, indicates a flow attachment close to the body-wing junction and still another distinct separation. Accordingly, it is difficult to conceive how one would produce a nonconical, nonlinear inviscid flow model that would describe such involved flow phenomena.

The nonslender delta wing with supersonic leading-edges has received considerable attention again recently by Whitehead[42] and by Cross and Hankey,[43] so that we will conclude this Section by making brief reference to the flow about a wing-body combination in hypersonic flow. Figure 23 shows regions of three-dimensional separation and attachment on the undersurface of a half-cone delta wing at $\alpha = 15°$ and $M_\infty = 12.6$. The boundary-layer flows are laminar. The transmitted shock from the cone produces separation on the delta wing inboard of the leading edge

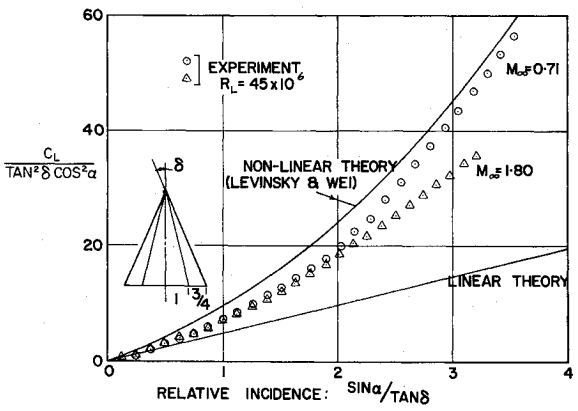

Fig. 21 Lift on 5° circular cone with 75% strake wings in subsonic and supersonic flow.

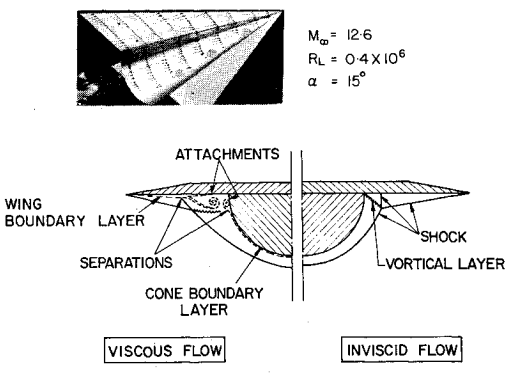

Fig. 23 Separation on underside of a half-cone delta wing in hypersonic flow.

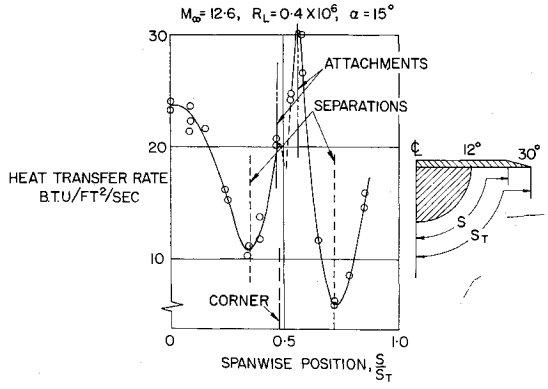

Fig. 24 Heat-transfer distribution on a half-cone delta wing.

and in addition, there is also a junction type separation. The high-local, heat-transfer rates at the flow attachment lines and the heat-transfer minima at the separation lines are shown on Fig. 24. More details of this study, which was carried out in the NAE hypersonic gun tunnel, are given in Ref. 44. Other extensive related hypersonic results from NASA Langley Research Center are described in Ref. 45.

Protuberance and "Favorable" Interaction Flows

Bluff Protuberances

There is an important class of three-dimensional viscous flows in which the initial two-dimensional (or axisymmetric) boundary layer suddenly meets a steep, adverse pressure gradient due to the blockage effect of a protuberance. The adverse nature of the pressure field relaxes as the flow proceeds around the obstruction, whether or not the obstruction is partially or wholly immersed within the boundary layer. Relative to the local external stream direction, the boundary layer first of all skews outwards in the adverse pressure field and then inwards upon encountering the favorable region. If the protuberance is sufficiently bluff, there will exist a three-dimensional separation region close to and about the junction of the protuberance with the surface.

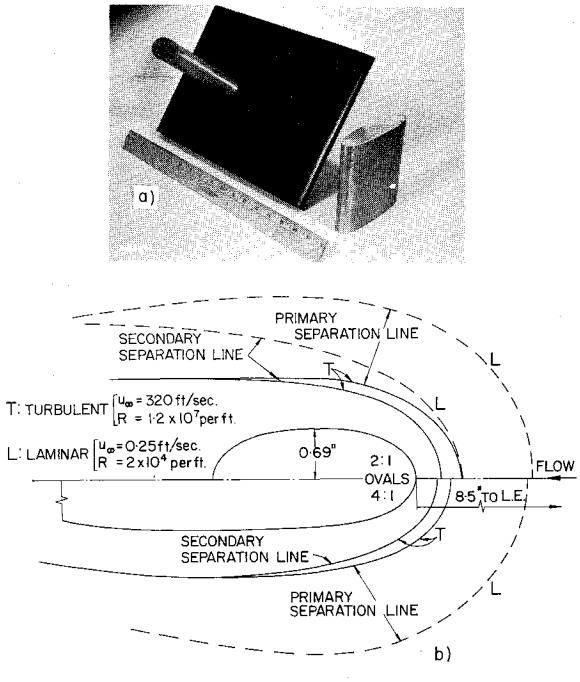

Fig. 25 Oval protuberances in subsonic flow: a) protuberance/flat plate model used in water tunnel and wind-tunnel tests: b) comparison between experimental laminar and turbulent flows about 2:1 and 4:1 oval cylinders.

Typical examples of bluff surface protuberances include wing leading edges at wing root/fuselage junctions, the foreparts of bulbous wheel housings, and boundary-layer diverters. As an example, East and Hoxey have commented[46] on the low-speed, boundary-layer effects in an "idealized" wing-body junction formed by an obstruction with a 1-ft radius nose, whose base was immersed in a turbulent boundary layer about 5.5 in. deep, and hence, of similar thickness to a boundary layer on a full-scale aircraft. Even though the shear layer resulting from the primary separation line about the base of the cylinder was seen to roll up within the depth of the undisturbed boundary layer (this observation was made previously in laminar flow studies in Refs. 30, 47, and 48) it appears that the surface static pressure distribution and local mainstream were distorted to an extent to indicate that these effects would be significant[10] in a practical wing-body junction. In this section, we shall attempt an outline of the flow about bluff protuberances, which when streamlined become satisfactory diversion systems for viscous flows.

The laminar boundary layer on a flat plate flowing about protuberances of either circular or Rankine oval section was investigated experimentally and analytically at the NAE.[47,48] It was shown that the initial line of three-dimensional separation about the cylinder—the primary separation line—could be predicted, to compare reasonably with experiment. In addition, these experiments in the NAE water tunnel facilitated an understanding of many of the complex flow phenomena downstream of the primary separation: in the region of secondary separation and roll-up of the shear layers.

The model that was used for the water tunnel experiments, Fig. 25, was subsequently sting-mounted in the NAE 5 × 5-ft wind tunnel, to compare the location of the three-dimensional separation lines in turbulent flow with those measured in laminar flow with both circular and oval section protuberances. As expected, the separation of the turbulent boundary layer was closer to the cylinder than in the laminar case, as exemplified by the flows

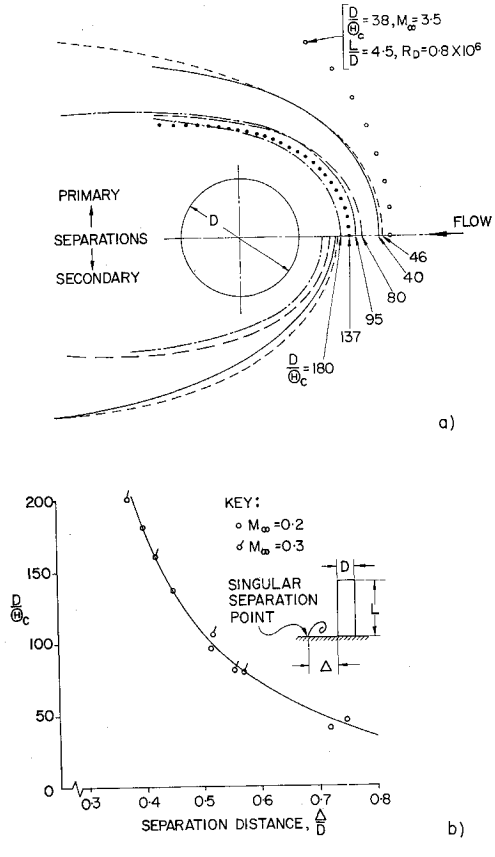

Fig. 26 Circular cylinder protuberances in subsonic flow: a) effect of D/Θ_c ratio upon separation line position with $L/D = 9$; b) dependence of separation distance Δ/D upon D/Θ_c ratio.

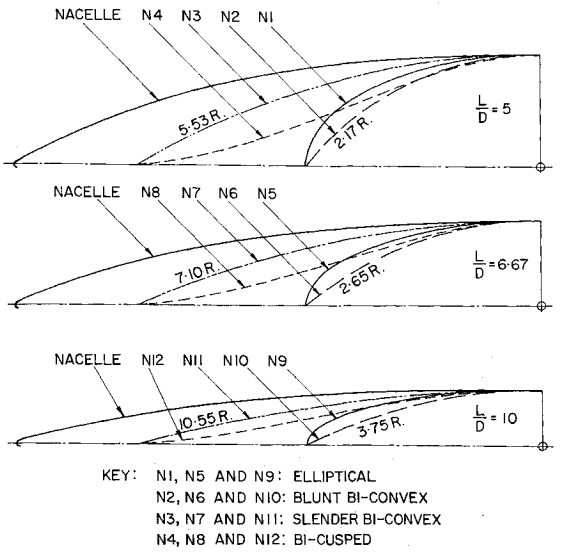

Fig. 27 Profiles of boundary-layer diverters used on drone at $M_\infty = 0.71$ and $R_L = 23 \times 10^6$.

about the 2:1 and 4:1 oval cylinders shown. The flat-plate had a span and chord of 9.8 and 14 in., with the cylinder axis set 10 in. from the leading edge. A range of circular cylinders, of length to diameter ratio L/D between 4.5 and 18, and diameter to undisturbed momentum deficit thickness of the boundary layer D/Θ_c between 40 and 200, was tested in turbulent flow. (Θ_c was calculated according to the wetted length of 10-in. recorded above.) The Reynolds number based on cylinder diameter spanned the range $0.2 \times 10^6 < R_T < 2.4 \times 10^6$, at Mach numbers of 0.2 and 0.3.

Figure 26 displays the tracings of the primary and secondary separation line positions, plotted to a base of unit cylinder diameter, for various ratios of D/Θ_c at $M_\infty = 0.2$ and $L/D = 9$. With decrease of D/Θ_c (i.e., decreasing D with respect to the same initial boundary layer) the primary and secondary separation line positions move away from the cylinder. Added to Fig. 26, is the position of a primary separation line about a cylinder in supersonic flow at $M_\infty = 3.51$,[49] tested at $R_D = 0.8 \times 10^6$, and hence, within the same Reynolds number range as the present subsonic experiments. It is perhaps fortuitous that the supersonic flow primary separation line position agrees with the trend established in subsonic flow (on the basis of D/Θ_c ratio) even though the L/D ratio is smaller (but not significantly so) and the mechanism of separation is due to the pressure rise generated by the bow shock wave of the cylinder.

Westkaemper concludes in a paper[50] on supersonic flow about circular section protuberances, that for cylinder L/D ratios greater than about 1, the distance of the singular separation point from the cylinder leading edge on the axis of symmetry Δ/D is virtually independent of L/D, D/Θ_c, M_∞, and R_D and equals $\Delta/D = 2.65$. One may see that this condition positions the primary separation upstream of the area shown on Fig. 26. This

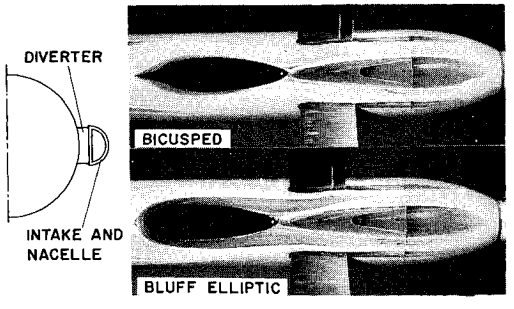

Fig. 28 Effect of boundary-layer diverter shape on three-dimensional separation at $M_\infty = 0.71$ and $R_L = 23 \times 10^6$.

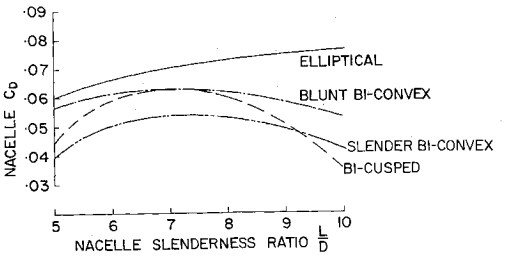

Fig. 29 Incremental drag of drone nacelle plus diverter at $M_\infty = 0.71$ and $R_L = 23 \times 10^6$.

independence is not seen in subsonic flow, because the protuberance adverse pressure field extends relatively much further upstream, although the separation itself is closer to the cylinder. The lower half of Fig. 26 is drawn to further emphasise the dependence of separation distance Δ/D upon the parameter D/Θ_c.

Diverters

The bluff protuberance flow provided an insight into how the design of a typical, turbulent boundary-layer diverter might be improved. As a consequence, a series of diverter flows was investigated,[51] situated beneath twin D-shaped intakes affixed to the body of a model surveillance drone. The various diverter planforms included elliptical, biconvex and bicusped shapes, attached to nacelles of three fineness ratios, $L/D = 5$, 6.67 and 10 (see Fig. 27).

Figure 28 demonstrates the improvement in diverter flow obtainable by changing the diverter geometry. This test was run at a freestream Mach number of 0.71 at a Reynolds number of 23 million based on the 3 ft length of the drone. The intake nacelles have been removed in the photographs to reveal the diverter shapes and the oil flow visualization on the drone body. Two boundary-layer diverter shapes are shown: a bluff, elliptical diverter that causes a large separation region about and downstream of the obstacle, and a more slender bicusped diverter which does not generate any significant separation. It is clear, therefore, that when designing boundary-layer diverters, one must avoid imposing large adverse streamwise pressure gradients upon the oncoming boundary layer such as those produced in stagnation point regions of bluff cylinders. (Notwithstanding, a recent illustration of the dorsal intake for one of the trijet airbus designs shows a diverter of the bluffest variety and one which is guaranteed to produce separation.)

Figure 29 displays the nacelle drag as a function of slenderness ratio L/D. Because the L/D ratio was achieved by varying the nacelle diameter, whilst maintaining a constant nacelle length, the drag increments attributable to mounting a nacelle plus diverter on the drone are based on the frontal area of the nacelle (including the diverter). No change of drag increment with Mach number was ascertained in the range $0.5 < M_\infty < 0.8$. We note that between the L/D limits of 5 and 10, the drag rises to a maximum and in the cases of the biconvex and bicusped diverters reduces again. The replacement of the elliptical boundary-layer diverter by either the slender biconvex or the bicusped diverter would give about a 30% reduction in total drag of the nacelle. Correspondingly, at $L/D = 5$, the slender biconvex diverter itself is about $\frac{2}{3}$ of the drag of the elliptical diverter, whereas at $L/D = 10$, the fraction improves to almost $\frac{1}{2}$. The biconvex diverter would probably be preferred to the bicusped in a practical installation because of its simpler shape and structure, and its improved performance at yaw.

It should be noted that the results of diverter tests in subsonic flow in Ref. 52 indicate that the drag changes were minor due to varying the diverter shape from simple wedge to a rounded nose wedge or to an ogee form. The lengths of the various diverters were all about the same with the consequence that the ogee was insufficiently slender. Evidently, the planform of the diverter must be chosen judiciously.

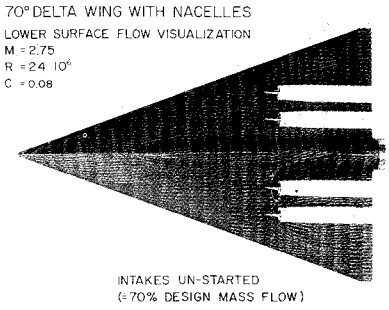

Fig. 30 Lower surface oil flow visualization on 70° delta wing with nacelles.

Interaction between Engine Nacelles and Adjacent Surfaces

Another viscous problem related to diverter flows occurs when designers attempt to take advantage of "favorable interference" effects, particularly on supersonic aircraft layouts.[53] Such favorable interference is always accompanied by local adverse pressure gradients that are superimposed upon the wing and fuselage boundary layers and which usually promote three-dimensional separations. Nichols[54] in discussing the interference between adjacent surfaces and a supersonic inlet flow appears to describe the role of the boundary layer only in a two-dimensional sense. Such a concept is totally inadequate to explain the interaction between the shock system from an unstarted inlet and an adjacent wing boundary layer, for example.

Figure 30 shows the oil dot flow visualization on the under-surface of a lifting 70° delta wing at $C_L = 0.08$ in a freestream flow of $M_\infty = 2.75$ and at a Reynolds number based on the maximum wing chord of 24 million. The four nacelle arrangement is typical in position and scale of a supersonic transport layout. The two uppermost intakes were operating at design mass flow with cone shock on lip. One will note a small region of three-dimensional separation caused by the wedge-shaped pylons (diverters) and cowl pressure field. The lower pair of intakes was throttled internally to about 70% design mass flow, forcing the throat normal shock outside of the cowl lip. The result of operating subcritically is to cause a massive three-dimensional separation of the starboard under-wing boundary layer, and high-local, heat-transfer rates in the reattachment regions downstream of the separation.[2] The accompanying changes in lift are shown in Fig. 31a. At a cruise lift coefficient of 0.08, occurring at an incidence angle of about 3° for this symmetrical wing, there is a 20% increase in lift from the throttling of the four intakes to 70% of the design mass flow; the corresponding increase in drag for subcritical operation is illustrated on Fig. 31b.

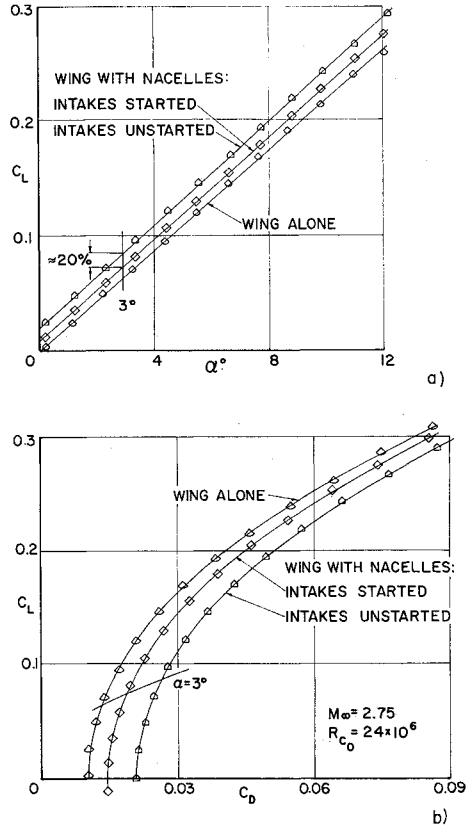

Fig. 31 70° delta wing with four nacelles at $M_\infty = 2.75$ and $R_{c_0} = 24 \times 10^6$: a) lift—incidence; b) lift-drag polars.

Another suitable example to summarise the interactions between viscous flow and diverter and propulsion intakes is the supersonic flow about a half-portion of an axisymmetric, conical intake situated adjacent to a fuselage.[55] The laminar three-dimensional separation caused by a slender half-cone mounted on a flat plate was studied in Ref. 56, where reasonable agreement was achieved between the calculated and measured separation line positions. The turbulent boundary-layer flow about a half-cone intake installation is qualitatively similar except that the adverse pressure field is now generated by the intake external shock wave system that impinges upon the thick boundary layers developing on the fuselage. If the viscous flows were ingested into the intake the efficiency of propulsion would be degraded, and the velocity distributions at the compressor face would suffer distortion. Accordingly, the intake is usually raised from the fuselage surface to permit both bleeding or/and diversion of the oncoming viscous flows.[57] A search of the literature (see the reports listed in Ref. 55) demonstrates that of the various tests performed on half-cone intakes or boundary bleed and diversion systems associated with partially submerged intakes, none has emphasized that the shock/boundary-layer interactions and separations are three-dimensional in character. Of some additional references noted here,[58-60] Ref. 60 perhaps came closest to "discovering" three-dimensional separation.

There is obvious difficulty in predicting the shock/boundary-layer interactions upon the fuselage and wing reflection planes, so that as an initial step, a simplified calculation of the partial cone flow itself was performed[55] (without the reflection planes) about a $\theta_c = 25°$ half-cone at Mach number 1.6. The pressure field that would be impressed upon the fuselage is approximately that existing between the shock wave and the half-cone (see Fig. 32). It is known that a turbulent boundary/layer negotiating a glancing oblique shock wave and subjected to a static pressure rise of 1.6 at $M_\infty = 1.6$, will skew, thicken, and eventually separate[61] from a three-dimensional separation line. That this indeed occurs in the intake case is confirmed by some oil flow

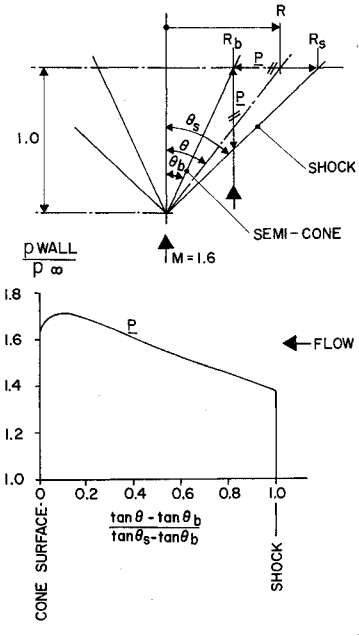

Fig. 32 Calculated pressures between shock wave and half-cone at $M_\infty = 1.6$.

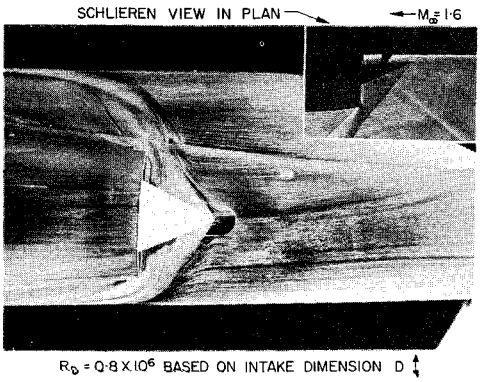

Fig. 33 Oil streak flow visualization about 25° half-cone intake on typical aircraft fuselage at $M_\infty = 1.6$ (after Culley[62]).

pictures taken by Culley[62] (typified by Fig. 33) about a half-cone intake of $\theta_c = 25°$, at $M_\infty = 1.6$ and at a Reynolds number of almost 1 million based upon the intake diameter of 2.08 in. An insert Schlieren photograph furnishes details of the cone shock and throat normal shock locations. The intake was operating at the design shock cone position and mass flow (apparently with spillage). The roll-up of the shear layers from the three-dimensional separation lines causes the upstream fuselage boundary layer to be diverted around the intake and allows the boundary-layer bleed scoops between the centre-body and the fuselage to receive only the higher momentum boundary-layer flow growing from the attachment region downstream of the three-dimensional separation.

Conclusion

Within the limits of our collective experience, we have attempted to demonstrate the importance of recognizing three-dimensional boundary-layer flows, and to illustrate some of the diverse kinds of three-dimensional separation that can occur on aircraft and missiles.

It is clear that greater efforts must be expended in the prediction of three-dimensional flowfields where there is a common intersection of the configuration components. Even if the inviscid interfering flows can be computed, there is currently no general method available to predict the growth, separation and roll-up of three-dimensional turbulent boundary layers.

References

[1] Howe, J. T., ed., *Some Fluid Mechanical Problems Related to Subsonic and Supersonic Aircraft,* NASA SP-183, 1968.

[2] Korkegi, R. H., "Survey of Viscous Interactions Associated with High Mach Number Flight," *AIAA Journal,* Vol. 9, No. 5, May 1971, pp. 771–784.

[3] Bauer, A. B., Smith, A. M. O., and Hess, J. L., "Potential Flow and Boundary Layer Theory as Design Tools in Aerodynamics," *CASI Journal,* Vol. 16, No. 2, Feb. 1970, pp. 53–69.

[4] Bagley, J. A., "Some Aerodynamic Principles for the Design of Swept Wings," *Progress in Aeronautical Sciences,* Vol. 3, Pergamon Press, New York, 1962, pp. 1–83.

[5] Hunt, G. K., "A Free-Flight Investigation of Wing-Body Junction Design for a Transonic Swept-Wing Aircraft," Current Paper 759, 1964, Aeronautical Research Council, U.K.

[6] Woodward, F. A., "Analysis and Design of Wing-Body Combinations at Subsonic and Supersonic Speeds," *Journal of Aircraft,* Vol. 5, No. 6, Nov.–Dec. 1968, pp. 528–534.

[7] Carmichael, R. L., Castellano, C. R., and Chen, C. F., "The Use of Finite Element Methods for Predicting the Aerodynamics of Wing-Body Combinations," *Analytic Methods in Aircraft Aerodynamics,* NASA SP-228, Oct. 1969, pp. 37–51.

[8] Woodward, F. A., Hunton, L. W., Gross, A. R., "A New Method for Calculating Near and Far Field Pressure about Arbitrary Configurations," *Analytic Methods in Aircraft Aerodynamics,* NASA SP-228, Oct. 1969, pp. 215–227.

[9] Levinsky, E. S., Wei, M. H. Y., and Maki, R. L., "Theoretical Studies of Vortex Flow on Slender Wing-Body Combinations," *Analytic Methods in Aircraft Aerodynamics,* NASA SP-228, Oct. 1969, pp. 113–129.

[10] Küchemann, D., "Some Remarks on the Interference Between a Swept Wing and a Fuselage," *Aerodynamic Interference, AGARD Conference Proceedings,* No. 71, Sept. 1970.

[11] Multhopp, H., "Aerodynamics of the Fuselage," TM 1036, Dec. 1942, NACA; translated from *Luftfahrtforschung,* Vol. 18, No. 2–3, March 29, 1941, Verlag von R. Oldenbourg, München und Berlin.

[12] Haines, A. B., "Subsonic Aircraft Drag: an Appreciation of Present Standards," Wind Tunnel Note 66, Nov. 1967, Aircraft Research Association, Bedford, U.K.

[13] Wickens, R. H., "Observations of the Vortex Wake of a Lifting Fuselage Similar to Those on Rear Loading Transport Aircraft," Aeronautical Rept. LR-395, Jan. 1964, National Research Council of Canada.

[14] Peake, D. J., "The Flows about Upswept Rear Fuselages of Typical Cargo Aircraft," DME/NAE Quarterly Bulletin No. 1968(3), Oct. 1968, National Research Council of Canada.

[15] Peake, D. J., "Three-Dimensional Flow Separations on Upswept Rear Fuselages," *CASI Journal,* Vol. 15, No. 10, Dec. 1969, pp. 399–408.

[16] Paterson, J. H., "Aerodynamic Design Features of the C-5A," *Aircraft Engineering,* Vol. 40, No. 6, June 1968, pp. 8–15.

[17] Taylor, C. R., Hall, J. R., and Hayward, R. W., "Super VC-10 Cruise Drag—A Wind Tunnel Investigation. Part I: Experimental Techniques," TR 69180, Aug. 1969, Royal Aircraft Establishment, U.K.

[18] De Santis, G. C. and Goodrick, T. F., "Wake Survey of Powered and Unpowered C-5A Aircraft Models," AIAA Paper 68-931, El Centro, Calif., 1968.

[19] Barnett, L. and Stevens, W. A., "Calculation of Pressure Distributions on Cambered Bodies of Arbitrary Cross-Section at Angle of Attack with Application to Transport Fuselage Afterbody Design," AIAA Paper 65-718, Los Angeles, Calif., 1965.

[20] Allen, H. J. and Perkins, E. W., "A Study of Effects of Viscosity on Flow over Slender Inclined Bodies of Revolution," Rept. 1048, 1951, NACA.

[21] Nettleton, T. R., "A Method of Estimating the Effect of Rear Fuselage Upsweep on Drag and Pitching Moment," Unpublished Internal Report, Nov. 1961, de Havilland Aircraft of Canada.

[22] Smith, J. H. B., "Improved Calculations of Leading-Edge Separation from Slender Delta Wings," TR 66070, March 1966, Royal Aircraft Establishment, U.K.; also *Proceedings of the Royal Society, Ser. A,* Vol. 306, 1968, pp. 67–90.

[23] Atraghji, E., "Surface Flow Visualisation, Surface Pressure and Surface Preston Tube Pitot Pressure Measurements over a 6:1 Ellipsoid at Incidence, at $M = 0.3$ and 0.74," NAE Data Rept. 5 × 5/0032, 1968, National Research Council of Canada.

[24] Preston, J. H., "The Determination of Turbulent Skin Friction by Means of Pitot Tubes," *Journal of Royal Aeronautical Society, U.K.,* Vol. 28, 1954, pp. 109–121.

[25] Thwaites, B., ed., *Incompressible Aerodynamics,* Chap. IX, Oxford University Press, England, 1960, pp. 369–418.

[26] Maruhn, K., "Druckverteilung auf den Zleichformig—Gradlining bewegten 3-Achsigen Ellipsoid Korper," *Forschungsbericht,* Nr. 1174, 1940.

[27] Robinson, A. and Laurmann, J. A., "Linearised Theory of Subsonic Flow," *Wing Theory,* Sec. 4.2, Cambridge University Press, England, 1956, pp. 316–319.

[28] Cloutier, M., "Etude de la Couche Limite Tridimensionnelle avec Flux de Chaleur," Ph.D. thesis, Aug. 1968, Laval Univ., Quebec, Canada.

[29] Matthews, C. W., "A Comparison of the Experimental Subsonic Pressure Distributions about Several Bodies of Revolution with Pressure Distributions Computed by Means of the Linearised Theory," TN 2519, Feb. 1952, NACA.

[30] Rainbird, W. J., Crabbe, R. S., Peake, D. J., and Meyer, R. F., "Some Examples of Separation in Three-Dimensional Flows," *CASI Journal,* Vol. 12, No. 10, Dec. 1966, pp. 409–423.

[31] Rainbird, W. J., "The External Flow Field about Yawed Circular Cones," *AGARD Conference Proceedings,* No. 30, May 1968.

[32] Rainbird, W. J., "Turbulent Boundary-Layer Growth and Separation on a Yawed Cone," *AIAA Journal,* Vol. 6, No. 12, Dec. 1968, pp. 2410–2416.

[33] Atraghji, E., "The Influence of Mach Number, Reynolds Number, Semi-Nose Angle and Roll Rate on the Development of Forces and Moments over a Series of Long Slender Bodies of Revolution at Incidence," NAE Data Rept. 5 × 5/0020, 1967, National Research Council of Canada.

[34] Ward, G. N., *Linearised Theory of Steady High Speed Flow*, Cambridge University Press, England, 1955, Chap. 9.

[35] Hoak, D. E., "Body Lift in the Non-Linear Angle-of-Attack Range," Sec. 4.2.12, Oct. 1960 (and revised Nov. 1965). USAF Stability and Control Datcom, Flight Control Div., Air Force Flight Dynamics Lab., Wright-Patterson Air Force Base, Ohio.

[36] Öhman, L. H., "A Surface Flow Solution and Stability Derivatives for Bodies of Revolution in Complex Supersonic Flow," Pts. I and II, Aeronautical Repts. LR-419, 519, Nov. and Dec. 1964, National Research Council of Canada.

[37] Atraghji, E., "Pressure Distribution over a Family of Inclined, Long Slender Bodies of Revolution at $M = 0.5$, 2.0 and 3.5," NAE Data Rept. $5 \times 5/0029$, 1968, National Research Council of Canada.

[38] Polhamus, E. C., "A Concept of the Vortex Lift of Sharp-Edge Delta Wings Based on a Leading-Edge-Suction Analogy," TN D-3767, Dec. 1966, NASA.

[39] Polhamus, E. C., "Applications of the Leading-Edge-Suction Analogy of Vortex Lift to the Drag due to Lift of Sharp-Edge Delta Wings," TN D-4739, Aug. 1968, NASA.

[40] Squire, L. C., Jones, J. G., and Stanbrook, A., "An Experimental Investigation of the Characteristics of Some Plane and Cambered 65° Delta Wings at $M = 0.7$ to 2.0," Rept. Aero 2655, July 1961, Royal Aircraft Establishment, U.K.

[41] Levinsky, E. S. and Wei, M. H. Y., "Non-Linear Lift and Pressure Distribution on Slender Conical Bodies with Strakes at Low Speeds," CR-1202, 1968, NASA.

[42] Whitehead, A. H., Jr. and Keyes, J. W., "Flow Phenomena and Separation over Delta Wings with Trailing-Edge Flaps at Mach 6," *AIAA Journal*, Vol. 6, No. 12, Dec. 1968.

[43] Cross, E. J., Jr. and Hankey, W. L., "Investigation of the Leeward Side of a Delta Wing at Hypersonic Speeds," *Journal of Spacecraft and Rockets*, Vol. 6, No. 2, Feb. 1969, pp. 185–190.

[44] Meyer, R. F. and Vaile, C. F., "An Experimental Study of the Hypersonic Flow about a Particular Half-Cone-and-Delta-Wing Lifting Configuration," Aeronautical Rept. LR-475, March 1967, National Research Council of Canada.

[45] Bertram, M. H. and Henderson, A., Jr., "Some Recent Research with Viscous Interacting Flow in Hypersonic Streams," *Proceedings of the 1969 Symposium on Viscous Interaction Phenomena in Supersonic and Hypersonic Flow*, University of Dayton Press, Ohio, 1970.

[46] East, L. F. and Hoxey, R. P., "Boundary Layer Effects in an Idealised Wing-Body Junction at Low Speed," TR 68161, July 1968, Royal Aircraft Establishment, U.K.

[47] Peake, D. J. and Galway, R. D., "Three-Dimensional Separation of a Plane, Incompressible, Laminar Boundary Layer Produced by a Circular Cylinder Mounted Normal to a Flat Plate," *Recent Developments in Boundary Layer Research*, Pt. 2, AGARDograph 97, pp. 1049–1080; also NAE Aeronautical Rept. LR-428, May 1965, National Research Council.

[48] Peake, D. J., Galway, R. D., and Rainbird, W. J., "The Three-Dimensional Separation of a Plane, Incompressible, Laminar Boundary Layer Produced by a Rankine Oval Mounted Normal to a Flat Plate," Aeronautical Rept. LR-446, Nov. 1965, National Research Council of Canada.

[49] Burbank P. B. and Newlander, R. A., "Heat Transfer and Pressure Measurements on a Flat Plate Surface and Heat Transfer Measurements on Attached Protuberances in a Supersonic Turbulent Boundary Layer at Mach Numbers of 2.65, 3.51 and 4.44," TN D-1372, Dec. 1962, NASA.

[50] Westkaemper, J. C., "Turbulent Boundary Layer Separation Ahead of Cylinders," *AIAA Journal*, Vol. 6, No. 7, July 1968, pp. 1352–1355.

[51] Peake, D. J., "Drag/Interference Studies on a Typical Cruciform Rear Wing Vehicle," NAE Data Rept. $5 \times 5/0012$, Dec. 1965, National Research Council of Canada.

[52] Daveport, C., "A Further Investigation of the Drag at Subsonic Speeds of Side Intake Boundary Layer Diverters," S & T Memo 7/68, Sept. 1968, British Ministry of Technology.

[53] Swan, W. C., "A Discussion of Selected Aerodynamic Problems on Integration of Propulsion Systems with the Airframe of Transport Aircraft," AGARDograph 103, Pt. I, Oct. 1965, pp. 23–68.

[54] Nichols, M. R., "Aerodynamics of Airframe-Engine Integration of Supersonic Aircraft," TN D-3390, Aug. 1966, NASA.

[55] Peake, D. J., Jones, D. J., and Rainbird, W. J., "The Half-Cone Flow and its Significance to Side-Mounted Intakes," *Aerodynamic Interference, AGARD Conference Proceedings*, No. 71, Sept. 1970.

[56] Shen, P. S. and Jones, D. J., "Three-Dimensional Laminar Boundary Layer Separation on a Flat Plate due to Flow Confrontation with a Half Cone at Incidence," Aeronautical Rept. LR-485, June 1967, National Research Council of Canada.

[57] Faro, I. D. V., *Supersonic Inlets*, AGARDograph 102, May 1965, pp. 121–123.

[58] Piercy, T. G. and Johnson, H. W., "Investigation at Mach Number 2.93 of Half of a Conical Spike Diffuser Mounted as a Side Inlet with Boundary Layer Control," RM E52G23, Sept. 1952, NACA.

[59] Piercy, T. G. and Johnson, H. W., "A Comparison of Several Systems of Boundary Layer Removal Ahead of a Typical Conical External Compression Side Inlet at Mach Numbers of 1.88 and 2.93," RM E53F16, Sept. 1953, NACA.

[60] Johnson, H. W. and Piercy, T. G., "Effect of Wedge-Type Boundary-Layer Diverters on Performance of Half-Conical Side Inlets at Mach Number 2.96," RM E54E20, 1954, NACA.

[61] Stalker, R. J., "Sweepback Effects in Turbulent Boundary Layer Shock Wave Interaction," *Journal of the Aerospace Sciences*, Vol. 27, No. 5, May 1960.

[62] Culley, M., "Annual Report of Department of Supply," 1966–1967, Aeronautical Research Labs., Melbourne, Australia.

[63] Peake, D. J., "Technical Evaluation Report on AGARD Specialists' Meeting on Aerodynamic Interference," AGARD-AR-34-71, May 1971.